Integrated Biodetection in a Nanofluidic Device

Liza Rassaei,[†,‡] Klaus Mathwig,[†,§] Shuo Kang,[†] Hendrik A. Heering,[∥] and Serge G. Lemay[†,*]

[†]MESA+ Institute for Nanotechnology, University of Twente, PO Box 217, 7500 AE, Enschede, The Netherlands, [‡]Department of Chemical Engineering, Delft University of Technology, Julianalaan 136, 2628 BL, Delft, The Netherlands, and [∥]Leiden Institute of Chemistry, Leiden University, PO Box 9502, 2300 RA, Leiden, The Netherlands. [§]Present address: (K. Mathwig) Institute for Integrative Nanosciences, IFW Dresden, Helmholtzstraße 20, 01069 Dresden, Germany.

ABSTRACT The sensing of enzymatic processes in volumes at or below the scale of single cells is challenging but highly desirable in the study of biochemical processes. Here we demonstrate a nanofluidic device that combines an enzymatic recognition element and electrochemical signal transduction within a six-femtoliter volume. Our approach is based on localized immobilization of the enzyme tyrosinase in a microfabricated nanogap electrochemical transducer. The enzymatic reaction product quinone is localized in the confined space of a nanochannel in which efficient redox cycling also takes place. Thus, the sensor allows the sensitive detection of minute amounts of product molecules generated by the enzyme in real time. This method is ideally suited for the study of ultra-small-volume systems such as the contents of individual biological cells or organelles.

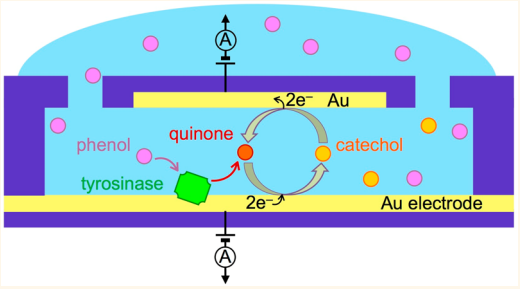

KEYWORDS: biosensors · bionanofluidic devices · electrochemistry · tyrosinase · nanobioanalytical systems

Downloaded via UNIV TWENTE on February 4, 2020 at 10:59:56 (UTC).
See https://pubs.acs.org/sharingguidelines for options on how to legitimately share published articles.

The interest in miniaturized bioanalytical systems based on micro- and nanofluidic devices[1−5] as sensitive and selective signal transduction elements continues to mount. This has led to a wide range of advances, from single-molecule DNA sizing[6−8] and size-deterministic particle sorting[9] to restriction mapping[10] and single-molecule DNA sequencing.[11,12] By comparison, relatively little progress has been made in miniaturizing electrochemical biosensors, which typically rely on the reactivity of a biological component for specificity, to the nanoscale. This is mainly due to the challenges of measuring the extremely low electrochemical currents generated by the activity of a minute number of enzyme molecules.

We have previously reported on nanofluidic electrochemical transducers[13] as an extension of classic thin-layer cells[14] with applications such as selective detection of paracetamol[15] and neurotransmitters[16] and as downstream detection elements in microscale analytical systems[17] or even as a detector of ultralow flows in nanochannels.[18,19] The capability of these nanogap devices to detect individual molecules has also been demonstrated.[20] Nanogap sensors exploit highly efficient redox cycling—namely, the repeated, successive reduction and oxidation of target molecules—to greatly amplify the faradaic signal from a (redox-active) analyte. This high intrinsic degree of amplification offers new opportunities for electrochemical sensors in which the intrinsic signal level would otherwise be too small for measurements. Moreover, these sensors directly yield an electric current proportional to the analyte concentration. Thus, the need for further signal transduction is eliminated.

Here we introduce a bionanofluidic sensing device in which all the elements of molecular recognition, signal transduction, and detection are integrated in a confined, femtoliter-scale reaction volume. The device consists of a microfabricated nanochannel in which are embedded both an enzyme and detection electrodes in a nanogap configuration. This geometry enables redox cycling and allows the continuous, real-time detection of the zeptomole (10^{-21} mol) amounts of product molecules generated by the enzymatic reaction.

An optical image of our microfabricated device is shown in Figure 1a. It consists of opposing planar microelectrodes separated by a thin, liquid-filled channel. The active region of the device consists of a volume

* Address correspondence to s.g.lemay@utwente.nl.

Received for review May 16, 2014 and accepted August 5, 2014.

Published online August 05, 2014
10.1021/nn502678t

© 2014 American Chemical Society

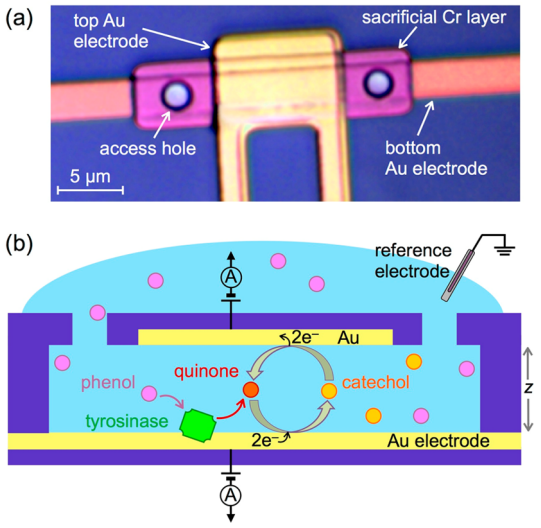

Figure 1. Nanofluidic bioelectrochemical detection. (a) Optical micrograph (top view) of a nanogap device. The active detection region is defined by the 10 μm × 3 μm area in which the two electrodes overlap. (b) Schematic principle of operation of the electrochemical bionanofluidic device: Immobilized tyrosinase enzymatically transforms inactive monophenolic substrate molecules into electrochemically active *o*-quinones. These molecules subsequently undergo redox cycling, yielding a highly amplified electrical current, thus enabling sensitive detection and direct signal transduction (channel height z = 200 nm).

enclosed by the two overlapping electrodes. In this report, we employ devices whose active volume has a length of 10 μm, a width of 3 μm, and a height of 200 nm, corresponding to a volume of 6 femtoliters. Because of the small electrode spacing, each product molecule travels several thousand times per second back and forth between the electrodes by diffusion. Since charge is transferred between the electrodes in each cycle, this redox cycling leads to a high amplification of the detected electrical charge per molecule.

As a prototypical recognition element, we use the protein tyrosinase, a copper-containing enzyme that is responsible for catalyzing the synthesis of melanin as well as other pigments. It is commonly used in electrochemical biosensors for the detection of phenolic compounds.[21−25] Thus, it has found applications in food inspection and medical diagnostics. Tyrosinase is able to bind dioxygen and catalyze the *ortho* hydroxylation of electrochemically inactive monophenols to electrochemically active *o*-diphenols (monooxygenase activity) as well as the oxidation of *o*-diphenols to the corresponding electrochemically active *o*-quinones (catechol oxidase activity) according to the following reaction:

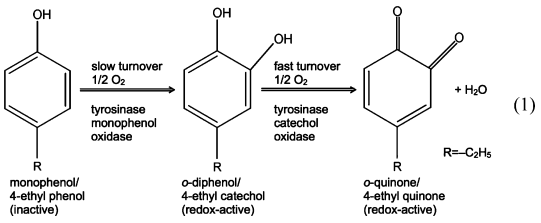

(1)

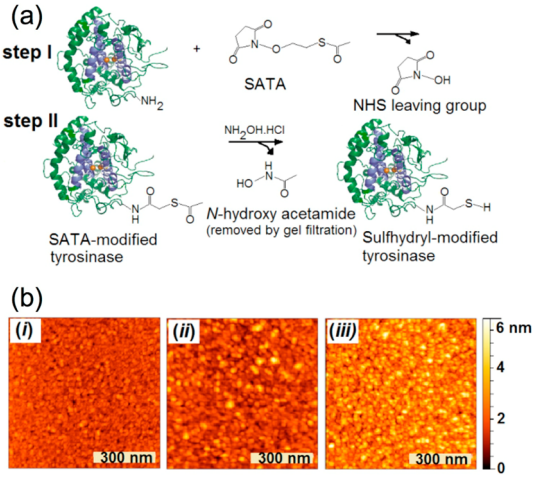

Figure 2. Enzyme immobilization. (a) Schematic illustration of the main steps for immobilization of tyrosinase on gold substrates. (b) Tapping mode AFM images of a macroscopic template-stripped gold electrode showing the surface density of tyrosinase (i) before enzyme immobilization, (ii) after 1 h of immobilization, and (iii) after 3 h of immobilization.

The principle of operation of our bionanofluidic sensor is schematically illustrated in Figure 1b. When the monophenolic substrate diffuses from the bulk reservoir into the nanochannel, it is transformed by the tyrosinase, which is bound homogeneously over the surface of the electrodes, into the redox-active enzymatic product, *o*-quinone. The latter is then detected electrochemically at the electrodes inside the nanochannel by redox cycling following a two-electron electrochemical reaction:

$$o\text{-quinone} + 2e^- + 2H^+ \leftrightarrows o\text{-diphenol} \qquad (2)$$

RESULTS AND DISCUSSION

Enzyme Immobilization. A key step in realizing this sensor is the immobilization of the enzyme tyrosinase on the Au electrodes in the nanochannel while retaining its catalytic activity. For this purpose, we developed a strategy based on addition of protected thiol groups to the enzyme using a bifunctional linker, *N*-succinimidyl *S*-acetylthioacetate (SATA). This consists of two consecutive steps, as sketched in Figure 2a. First, the primary amines on tyrosinase react with the linker *via* a nucleophilic attack to form an amide bond. Second, hydroxylamine-hydrochloric acid is used to deprotect the linker and generate a free thiol group, which is reactive to gold surfaces.

In order to test this immobilization approach, the thiol-functionalized tyrosinase was first immobilized on gold substrates prepared by template stripping to yield a flat surface.[26] Figure 2b shows typical atomic force microscopy (AFM) images of gold substrates before and after the immobilization of tyrosinase. Enzyme molecules are clearly visible on the gold surface after immobilization as globular structures that increase the roughness of the surface (from

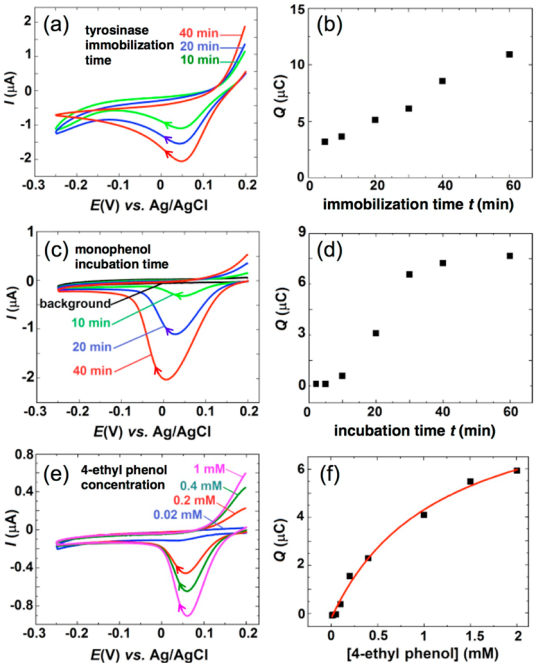

Figure 3. Enzymatic activity of immobilized tyrosinase. (a) Cyclic voltammograms (scan rate: 10 mV s^{-1}) for the reduction of 4-ethylquinone generated in a 2 mM solution of 4-ethylcatechol in 0.2 M phosphate buffer solution, pH = 6.8, for different tyrosinase immobilization times on a 1.6 mm diameter gold electrode. (b) Cathodic peak charge in (a) *versus* tyrosinase immobilization time. (c) Cyclic voltammograms (scan rate: 20 mV s^{-1}) for the reduction of 4-ethylquinone generated at a tyrosinase-modified gold electrode of 3 mm diameter in a thin-layer cell from a 2 mM solution of 4-ethylphenol in a 0.2 M phosphate buffer solution. The voltammograms are shown as a function of phenol incubation time for a fixed tyrosinase immobilization time of 2 h. (d) Cathodic peak charge in (c) *versus* 4-ethylphenol incubation time. (e) Cyclic voltammograms (scan rate: 10 mV s^{-1}) for reduction of 4-ethylquinone under the same conditions as in (c) for different concentrations of 4-ethylphenol (phenol substrate incubation time of 30 min). (f) Cathodic peak charge in (e) *versus* 4-ethylphenol concentrations. The solid line is a guide to the eye that follows the functional form appropriate for Michaelis–Menten kinetics.

1.74 ± 0.02 nm to 1.83 ± 0.10 and 2.55 ± 0.09 nm after 1 and 3 h incubation, respectively). Figure 2b(ii) and (iii) further show that the enzyme surface coverage increases as the immobilization time is prolonged from 1 h to 3 h.

Evaluation of Enzyme Activity. Having established the tyrosinase immobilization procedure, we evaluated the activity of the immobilized enzymes using electrochemical methods. As a first test, we studied the activity of the enzyme for a substrate, 4-ethylcatechol, with a high turnover rate of ~8×10^2 s^{-1} into 4-ethylquinone.[27−29] This high rate allows detecting the enzymatic product using conventional voltammetry. This is in contrast to monophenolic compounds, which are our ultimate target, as they exhibit turnover rates of only 14 molecules per second per enzyme.[30] We immobilized the enzyme on a 1.6 mm diameter gold disk electrode and performed cyclic voltammetry. Figure 3a shows typical cyclic voltammograms for the reduction of 4-ethylquinone generated in an enzymatic reaction at the electrode surface from a solution of 2 mM 4-ethylcatechol in 0.2 M phosphate buffer (pH = 6.8) for a variety of enzyme incubation times. The electrode potential was swept from 0.2 V to −0.25 V *versus* Ag/AgCl and back. A cathodic peak for reduction of 4-ethylquinone was clearly observed with an onset at 0.14 V *versus* Ag/AgCl. The current for the reduction of the 4-ethylquinone product increases with longer enzyme immobilization times. The charge under the cathodic peak current corresponds to the amount of 4-ethylquinone produced at the electrode surface. When plotting the charge under the cathodic peak current *versus* the tyrosinase immobilization time (Figure 3b), a linear behavior is observed. This demonstrates that enzyme molecules retain their catalytic activity after immobilization and that the concentration of active enzymes on the surface increases with the time of immobilization. This observation is consistent with the AFM measurements.

Monophenolase Activity. The monophenolase activity of immobilized tyrosinase has an ~50 times slower turnover rate compared to its diphenolase activity. To study this activity, we generated measurable amounts of enzymatic product by prolonged incubation in a closed volume. We used a 3 mm diameter gold disk electrode that formed part of a conventional electrochemical thin-layer cell. The gold working electrode was enclosed by a gasket of thickness 12.7 μm, yielding a thin-layer cell volume of 9×10^{-11} m^3 (90 nL). Tyrosinase was immobilized for 2 h on the electrode, and the cell was then incubated with a solution of 2 mM 4-ethylphenol in 0.2 M phosphate buffer, pH = 6.8, for varied times ranging from 10 to 40 min. These substrate incubation times allowed the enzyme to generate larger amounts of product to be subsequently detected in a voltammetric sweep. Figure 3c shows cyclic voltammograms for the reduction of 4-ethylquinone produced by the tyrosinase enzymatic reaction following different 4-ethylphenol incubation times. Increasing the incubation time clearly increases the magnitude of the reduction current of 4-ethylquinone.

In a quantitative analysis, Figure 3d shows the charge under the cathodic peak as a function of the incubation time. This charge increases with incubation times of up to 30 min and then levels off. This saturation indicates that almost all of the substrate in the thin-layer cell in the vicinity of the electrode has been turned over to the product 4-ethylquinone. For a 30 min incubation time, the charge under the peak is 7 μC. As each molecule of 4-ethylquinone contributes two electrons to the current and by assuming an average turnover rate of ~14 s^{-1} per enzyme,[30] we can estimate the number of active immobilized enzymes on the gold electrode to be ~10^9. Considering that tyrosinase has dimensions 4.0 × 5.5 × 6.0 nm^3,[31] this

corresponds to an *active* enzyme surface coverage of about 0.25%.

As a final control, Figure 3e shows cyclic voltammograms for different 4-ethylphenol substrate concentrations at a fixed substrate incubation time of 30 min, also obtained with the thin-layer cell. The cathodic current for reduction of 4-ethylquinone increases with increasing 4-ethylphenol concentration, showing that the rate of conversion into 4-ethylquinone is the main limiting factor. In Figure 3f the charge under the cathodic peak for reduction of 4-ethylquinone *versus* the substrate concentration is shown. This function follows Michaelis–Menten kinetics, represented by the solid red line. This is expected since the integrated charge is directly related to the turnover rate of the enzyme; a more quantitative comparison is however impossible here due to the poorly defined mass transport within the thin-layer cell on these long time scales.

Enzymatic Phenol Detection in Nanochannels. Having established the viability of the experimental procedure for immobilizing tyrosinase, we proceeded to measurements in the nanogap devices. For this purpose, tyrosinase was immobilized in the nanofluidic channel for 2 h by placing a reservoir containing the tyrosinase solution onto the surface of the nanogap chip. The nanochannel geometry does not limit the one-dimensional diffusive transport of the enzyme to the surface of the electrodes, considering that a protein of the size of tyrosinase diffuses over a distance of 10 μm within seconds.

Figure 4a shows cyclic voltammograms for the tyrosinase-modified nanofluidic sensors for a 0.2 M phosphate buffer solution (background signal, red lines) and in the presence of 0.5 mM 4-ethylphenol (blue lines) obtained by sweeping the top electrode while keeping the bottom electrode at a reducing potential for quinone (0 V *versus* Ag/AgCl). While the background signal is featureless, a clear sigmoidal wave is observed at 0.3 V *versus* Ag/AgCl in the presence of phenol. This signal at the two electrodes is of equal magnitude and of opposite sign, a key signature of redox cycling. Moreover, at high overpotentials the two signals clearly show anticorrelated current fluctuations, which is a characteristic for redox cycling in nanogap sensors caused by statistical fluctuations of the number of molecules.[13] We therefore attribute this wave to redox cycling of the 4-ethylquinone product resulting from the monophenolase activity of tyrosinase on 4-ethylphenol. We emphasize an important difference between this observation and that of Figure 3c and e: in the conventional thin-layer cell the measurement requires a long incubation time (due to the low enzymatic turnover rate), during which the product is accumulated. The incubation is then followed by a one-shot measurement. In the nanogap sensor the presence of phenol results in an instantaneous steady-state current due to the sensitive

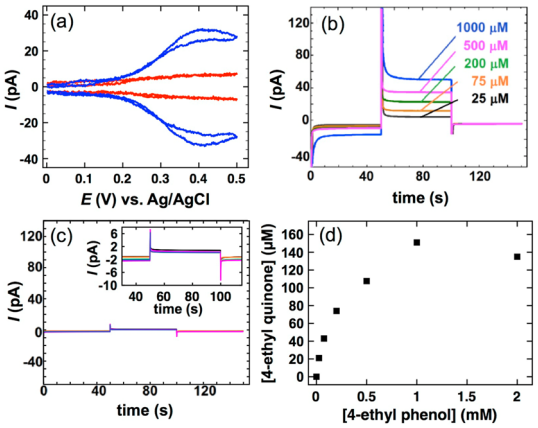

Figure 4. Phenol detection in nanogap devices. (a) Cyclic voltammograms for 0.2 M phosphate buffer solution, pH = 6.8, in the absence (background, red) and presence of 0.5 mM 4-ethylphenol (blue). The top electrode was swept at 10 mV s^{-1}, while the potential of the bottom electrode was kept at a constant potential of 0 V *versus* Ag/AgCl (top curves: oxidation current at top electrodes). (b) Chronoamperometric measurements (bottom electrode) for different concentrations of 4-ethylphenol. The potential of the bottom electrode is stepped between 0 and 0.5 V *versus* Ag/AgCl every 50 s, while the potential of the top electrode is kept at a constant potential of 0 V *versus* Ag/AgCl. Variation in the resulting current reflects changes of the phenol concentration within the 6 fL measurement volume. (c) Corresponding chronoamperometric results for a 0.2 M phosphate buffer solution with the same conditions as in (b) but without tyrosinase. (The inset zooms in on the current step.) (d) Concentration of 4-ethylquinone produced by the enzymatic reaction in the device *versus* the concentration of the 4-ethylphenol substrate.

detection of the redox-active product. This current can be followed in real time. In this steady state, each enzyme molecule inside the nanochannel produces a stream of product molecules at a given rate. Each product molecule then undergoes redox cycling inside the nanochannel, generating an amplified current until its random diffusive trajectory brings it to an access hole of the device, through which it exits into the external reservoir.

In order to quantitatively investigate the electrochemical properties of the device, we performed chronoamperometric experiments. For this purpose, we biased the top electrode at a fixed potential of 0 V *versus* Ag/AgCl and stepped the potential of the bottom electrode from 0 to 0.5 V *versus* Ag/AgCl for 50 s. This switching between the non-redox cycling and redox cycling conditions allows compensating for any residual drift or offset in the measured signal. Figure 4b shows the results obtained in this experiment for different concentrations of 4-ethylphenol. Each curve is an average of eight consecutive steps so as to minimize the effect of instrumental drift (see Supporting Figure S1 for raw current–time traces). The short transient response[32,33] toward the steady-state current upon the current step to cycling conditions is largely caused by the resistance-capacitance (RC) charging time of the stepped electrode. The steady-state

redox-cycling current increases with increasing substrate concentration, as expected and desired for a real-time amperometric sensor.

Control experiments were carried out to further verify that the observed catalytic response is indeed caused by the presence of tyrosinase in the nanochannel and not due to catalytic properties of the gold electrodes. Figure 4c shows the results of chronoamperometry performed under the same conditions as in Figure 4b but in the absence of tyrosinase on the electrodes. The observed current is much lower than the redox cycling current and is independent of substrate concentration, unambiguously proving that the current observed in the presence of the enzyme is caused solely by the catalytic activity of tyrosinase.

In order to calibrate the amount of quinone produced in the nanochannel for each concentration, we recorded the redox-cycling current as a function of the 4-ethylcatechol concentration (Supporting Figure S2). This allows converting the current values observed in the amperometric experiments into corresponding product concentrations. Figure 4d shows the concentration of 4-ethylquinone produced by the enzymatic reaction as a function of 4-ethylphenol concentration. The generated signal depends linearly on the 4-ethylphenol concentration at low concentrations, but saturates around 1 mM of 4-ethylphenol. This is consistent with the observed dependence of the enzymatic turnover rate on the concentration of 4-ethylphenol following Michaelis–Menten kinetics.[30] These data further show that the enzyme remains active during measurements conducted over the course of 36 h involving multiple changes of sample solution.

The concentration of the quinone/catechol redox couple in the nanofluidic channel results from the balance between two opposing rates: the rate of production of quinone, which is set by the active enzyme density and turnover rate, and the rate at which the product molecules exit the nanogap by diffusion. The fact that the quinone product concentration is much smaller than that of the phenol substrate indicates that mass transport very effectively withdraws product molecules from the device. Conversely, this also shows that mass transport of phenol *into* the nanogap is not a limiting factor on the overall turnover rate. The activity of the enzyme itself therefore dominates the observed signal, the optimal scenario for any biosensor.

CONCLUSIONS

We have established a new functionality in electrochemical nanofluidic devices by introducing molecular recognition *via* an enzymatic system. This involved in particular devising and validating a new protocol for immobilization of tyrosinase at metal electrodes. The result is a biosensing device that encapsulates both recognition and signal transduction in a femtoliter-scale volume. Here the lowest measured phenol concentration of 25 μM corresponds to only 150 zeptomoles of substrate molecules in the nanochannel detection area and to only about 120 zeptomoles, or 70 000 molecules, of the quinone/catechol product. Moreover, we can fully capitalize on the high signal amplification of the sensor, as it is not necessary to accumulate product by prolonged incubation in spite of the slow enzymatic turnover. Instead, the direct real-time detection of the enzymatic activity is possible, also without the need for complex signal transduction, as the molecules conveniently and directly generate a current.

The use of an enzyme as recognition element is not limited to tyrosinase. The only requirement is that the redox properties (redox potential, electron transfer kinetics) of the substrate molecule to be recognized and the enzymatic product differ sufficiently to yield a difference in electrochemical signal. This differential response can be optimized by selection of electrode potential windows. Modification of the electrode surfaces and choice of metal can also be used as a secondary molecular affinity selection strategy. Such strategies are commonly used for electrochemical sensors. However, these often yield only partial selectivity. Adding a biological primary recognition element will reduce the common electrochemical specificity problem to a selection between only a few (ideally two) molecular species from a complex mixture.

Our approach is particularly well suited for studying small-volume samples. The volume of the device is sufficiently small to study the content of an individual biological cell, ranging from large eukaryotic oocytes to submicrometer bacteria. We further anticipate that sensitivity can be greatly improved[20] with further optimization. By reducing the electrode spacing to about 40 nm to boost signal strength and by reducing the number of immobilized enzyme molecules (currently ~5000 active molecules), it will become possible to electrochemically explore enzyme kinetics at the single-molecule level.

METHODS

Immobilization of Tyrosinase. An 8 mg amount of *N*-succinimidyl *S*-acetylthioacetate was dissolved in 500 μL of DMSO. Then 10 μL of this solution was added to a 1 mL solution of 60 μM tyrosinase. The contents were mixed at room temperature. After 30 min, the reaction mixture was added to a dextran desalting column to remove unreacted reagents. To proceed further, SATA-modified enzymes were mixed with 100 μL of deacetylation solution (a mixture of 0.5 M hydroxylamine and 25 mM EDTA) for 2 h at room temperature. The content was

subsequently added to a dextran desalting column to purify the SATA-modified enzyme from the hydroxylamine in deacetylation solution. After collection, the modified protein with a free thiol group was ready to be immobilized on the gold surface.

Device Fabrication. Nanofluidic sensors were fabricated as described previously,[19,32] except that Au instead of Pt electrodes were deposited. In brief, on a 100 mm Si wafer isolated with 500 nm thick thermally grown SiO_2, a 20 nm thick gold bottom electrode, a 200 nm Cr sacrificial layer, and a 100 nm thick gold top electrode were sequentially deposited by electron-beam evaporation and patterned using a lift-off process based on a positive photoresist (OIR 907-17, Arch Chemicals). The thickness of the Cr layer determined the nominal height of the channel. Afterward, a passivation layer consisting of 90 nm/325 nm/90 nm thick SiO_2/SiN/SiO_2 was deposited by plasma-enhanced chemical vapor deposition. The high temperature employed in this process (300 °C) caused roughing of the Au/Cr interface. Access holes were then etched through the passivation layer using reactive ion etcher, reaching the Cr sacrificial layer. Finally, the sacrificial layer was etched by wet Cr etchant at room temperature, creating a nanochannel. A reservoir in polydimethylsiloxane was placed onto the chip to connect the nanochannel with solutions containing tyrosinase and phenol.

Electrical Measurements. Conventional electrochemical experiments were performed in a three-electrode cell system using a CHI832 bipotentiostat. A conventional electrochemical microscale thin-layer cell with a 3 mm diameter gold disc electrode and a spacer gasket thickness of 12.7 μm was obtained from BASi. Amperometric experiments in the thin-layer cell employed the same measurement system but with a second working electrode (three four-electrode configuration). Low-current measurements in nanogap devices were carried out using a three-electrode system (no counter electrode is used due to the extremely low currents at the reference electrode) consisting of two Keithley 6430 subfemtoamp remote source meters, used both as voltage sources to bias the electrode potentials and as current-detection elements. A 3 M Ag/AgCl electrode (BASi) was used as reference electrode. All the experiments were carried out at 20 $\pm$ 2 °C. AFM measurements were carried out using a DI AFM Nanoscope Dimension 3100 in tapping mode.

Conflict of Interest: The authors declare no competing financial interest.

Supporting Information Available: Chemical reagents, raw current−time traces for phenol detection in the nanochannel, calibration of quinone in the nanochannel. This material is available free of charge *via* the Internet at http://pubs.acs.org.

Acknowledgment. We thank Kim Sweers for help with preparation of template-stripped gold surfaces and Martin Siekman for assistance with AFM studies. We further gratefully acknowledge the financial support from The Netherlands Organization for Scientific Research (NWO) and the European Research Council (ERC).

REFERENCES AND NOTES

1. Kovarik, M. L.; Jacobson, S. C. Nanofluidics in Lab-on-a-Chip Devices. *Anal. Chem.* **2009**, *81*, 7133–7140.
2. Rassaei, L.; Singh, P. S.; Lemay, S. G. Lithography-Based Nanoelectrochemistry. *Anal. Chem.* **2011**, *83*, 3974–3980.
3. Arayanarakool, R.; Shui, L.; Kengen, S. W.; Van Den Berg, A.; Eijkel, J. C. Single-Enzyme Analysis in a Droplet-Based Micro- and Nanofluidic System. *Lab Chip* **2013**, *13*, 1955–1962.
4. Rothberg, J. M.; Hinz, W.; Rearick, T. M.; Schultz, J.; Mileski, W.; Davey, M.; Leamon, J. H.; Johnson, K.; Milgrew, M. J.; Edwards, M. An Integrated Semiconductor Device Enabling Non-Optical Genome Sequencing. *Nature* **2011**, *475*, 348–352.
5. Sackmann, E. K.; Fulton, A. L.; Beebe, D. J. The Present and Future Role of Microfluidics in Biomedical Research. *Nature* **2014**, *507*, 181–189.
6. Han, J.; Craighead, H. G. Separation of Long DNA Molecules in a Microfabricated Entropic Trap Array. *Science* **2000**, *288*, 1026–1029.
7. Sen, Y.-H.; Jain, T.; Aguilar, C. A.; Karnik, R. Enhanced Discrimination of DNA Molecules in Nanofluidic Channels through Multiple Measurements. *Lab Chip* **2012**, *12*, 1094–1101.
8. Chan, E. Y.; Goncalves, N. M.; Haeusler, R. A.; Hatch, A. J.; Larson, J. W.; Maletta, A. M.; Yantz, G. R.; Carstea, E. D.; Fuchs, M.; Wong, G. G. DNA Mapping Using Microfluidic Stretching and Single-Molecule Detection of Fluorescent Site-Specific Tags. *Genome Res.* **2004**, *14*, 1137–1146.
9. Huang, L. R.; Cox, E. C.; Austin, R. H.; Sturm, J. C. Continuous Particle Separation through Deterministic Lateral Displacement. *Science* **2004**, *304*, 987–990.
10. Riehn, R.; Lu, M.; Wang, Y.-M.; Lim, S. F.; Cox, E. C.; Austin, R. H. Restriction Mapping in Nanofluidic Devices. *Proc. Natl. Acad. Sci. U.S.A.* **2005**, *102*, 10012–10016.
11. Marie, R.; Kristensen, A. Nanofluidic Devices towards Single DNA Molecule Sequence Mapping. *J. Biophotonics* **2012**, *5*, 673–686.
12. Aguilar, C. A.; Craighead, H. G. Micro-and Nanoscale Devices for the Investigation of Epigenetics and Chromatin Dynamics. *Nat. Nanotechnol.* **2013**, *8*, 709–718.
13. Zevenbergen, M. A.; Krapf, D.; Zuiddam, M. R.; Lemay, S. G. Mesoscopic Concentration Fluctuations in a Fluidic Nanocavity Detected by Redox Cycling. *Nano Lett.* **2007**, *7*, 384–388.
14. Daruhazi, L.; Tokuda, K.; Farsang, G. Cyclic Voltammetry for Reversible Redox-Electrode Reactions in Thin-Layer Cells with Closely Separated Working and Auxiliary Electrodes of the Same Size. *J. Electroanal. Chem. Interfacial Electrochem.* **1989**, *264*, 77–89.
15. Goluch, E. D.; Wolfrum, B.; Singh, P. S.; Zevenbergen, M. A.; Lemay, S. G. Redox Cycling in Nanofluidic Channels Using Interdigitated Electrodes. *Anal. Bioanal. Chem.* **2009**, *394*, 447–456.
16. Wolfrum, B.; Zevenbergen, M.; Lemay, S. Nanofluidic Redox Cycling Amplification for the Selective Detection of Catechol. *Anal. Chem.* **2008**, *80*, 972–977.
17. Rassaei, L.; Mathwig, K.; Goluch, E. D.; Lemay, S. G. Hydrodynamic Voltammetry with Nanogap Electrodes. *J. Phys. Chem. C* **2012**, *116*, 10913–10916.
18. Mathwig, K.; Mampallil, D.; Kang, S.; Lemay, S. G. Electrical Cross-Correlation Spectroscopy: Measuring Picoliter-per-Minute Flows in Nanochannels. *Phys. Rev. Lett.* **2012**, *109*, 118302.
19. Mathwig, K.; Lemay, S. G. Pushing the Limits of Electrical Detection of Ultralow Flows in Nanofluidic Channels. *Micromachines* **2013**, *4*, 138–148.
20. Kang, S.; Nieuwenhuis, A. F.; Mathwig, K.; Mampallil, D.; Lemay, S. G. Electrochemical Single-Molecule Detection in Aqueous Solution Using Self-Aligned Nanogap Transducers. *ACS Nano* **2013**, *7*, 10931–10937.
21. Ortega, F.; Domínguez, E.; Burestedt, E.; Emnéus, J.; Gorton, L.; Marko-Varga, G. Phenol Oxidase-Based Biosensors as Selective Detection Units in Column Liquid Chromatography for the Determination of Phenolic Compounds. *J. Chromatogr. A* **1994**, *675*, 65–78.
22. Önnerfjord, P.; Emnéus, J.; Marko-Varga, G.; Gorton, L.; Ortega, F.; Domínguez, E. Tyrosinase Graphite-Epoxy Based Composite Electrodes for Detection of Phenols. *Biosens. Bioelectron.* **1995**, *10*, 607–619.
23. Nistor, C.; Emnéus, J.; Gorton, L.; Ciucu, A. Improved Stability and Altered Selectivity of Tyrosinase Based Graphite Electrodes for Detection of Phenolic Compounds. *Anal. Chim. Acta* **1999**, *387*, 309–326.
24. Ortega, F.; Dominguez, E.; Jönsson-Pettersson, G.; Gorton, L. Amperometric Biosensor for the Determination of Phenolic Compounds Using a Tyrosinase Graphite Electrode in a Flow Injection System. *J. Biotechnol.* **1993**, *31*, 289–300.
25. Burestedt, E.; Narvaez, A.; Ruzgas, T.; Gorton, L.; Emnéus, J.; Domínguez, E.; Marko-Varga, G. Rate-Limiting Steps of Tyrosinase-Modified Electrodes for the Detection of Catechol. *Anal. Chem.* **1996**, *68*, 1605–1611.
26. Hegner, M.; Wagner, P.; Semenza, G. Ultralarge Atomically Flat Template-Stripped Au Surfaces for Scanning Probe Microscopy. *Surf. Sci.* **1993**, *291*, 39–46.

27. Fenoll, L. G.; Rodríguez-López, J. N.; García-Sevilla, F.; García-Ruiz, P. A.; Varón, R.; García-Cánovas, F.; Tudela, J. Analysis and Interpretation of the Action Mechanism of Mushroom Tyrosinase on Monophenols and Diphenols Generating Highly Unstable *o*-Quinones. *Biochim. Biophys. Acta, Protein Struct. Mol. Enzymol.* **2001**, *1548*, 1–22.
28. Espín, J. C.; Varón, R.; Fenoll, L. G.; Gilabert, M.; García-Ruíz, P. A.; Tudela, J.; García-Cánovas, F. Kinetic Characterization of the Substrate Specificity and Mechanism of Mushroom Tyrosinase. *Eur. J. Biochem.* **2000**, *267*, 1270–1279.
29. Muñoz-Muñoz, J. L.; García-Molina, M. del M.; Garcia-Molina, F.; Berna, J.; Garcia-Ruiz, P. A.; García-Moreno, M.; Rodriguez-Lopez, J. N.; Garcia-Canovas, F. Catalysis and Inactivation of Tyrosinase in Its Action on *o*-Diphenols, *o*-Aminophenols and *o*-Phenylendiamines: Potential Use in Industrial Applications. *J. Mol. Catal. B: Enzym.* **2013**, *91*, 17–24.
30. Rassaei, L.; Cui, J.; Goluch, E. D.; Lemay, S. G. Substrate-Dependent Kinetics in Tyrosinase-Based Biosensing: Amperometry *vs*. Spectrophotometry. *Anal. Bioanal. Chem.* **2012**, *403*, 1577–1584.
31. Ismaya, W. T.; Rozeboom, H. J.; Weijn, A.; Mes, J. J.; Fusetti, F.; Wichers, H. J.; Dijkstra, B. W. Crystal Structure of Agaricus Bisporus Mushroom Tyrosinase: Identity of the Tetramer Subunits and Interaction with Tropolone. *Biochemistry (Moscow)* **2011**, *50*, 5477–5486.
32. Kang, S.; Mathwig, K.; Lemay, S. G. Response Time of Nanofluidic Electrochemical Sensors. *Lab Chip* **2012**, *12*, 1262.
33. Mathwig, K.; Lemay, S. G. Mass Transport in Electrochemical Nanogap Sensors. *Electrochim. Acta* **2013**, *112*, 943–949.